Magnetization reversal of submicrometer Co rings with uniaxial anisotropy via scanning magnetoresistance microscopy

Xiaoyong Liu,[1] D. Mazumdar,[1] B. D. Schrag,[1,2] W. Shen,[1] and Gang Xiao[1]
[1]*Physics Department, Brown University, Providence, Rhode Island 02912, USA*
[2]*Micro Magnetics, Inc., 151 Martine Street, Fall River, Massachusetts 02723, USA*
(Received 17 November 2003; revised manuscript received 1 April 2004; published 9 July 2004)

We have investigated the magnetization reversal mechanism of narrow submicrometer Co rings using scanning magnetoresistance microscopy. Thermal annealing in a magnetic field introduced a uniaxial anisotropy and significant structural changes in the samples. We have observed a complicated multidomain state at intermediate field ranges, and onion states at saturation, for samples annealed in a field. This observation is in contrast to the flux-closed vortex state for unannealed rings. Micromagnetic simulations have shown that the switching occurs through a gradual noncoherent buckling-like reversal process followed by coherent rotation.

DOI: 10.1103/PhysRevB.70.014407 PACS number(s): 75.75.+a, 75.60.−d, 85.75.−d

I. INTRODUCTION

Advances in microfabrication techniques, such as electron-beam,[1] interference,[2] and nanoimprint lithography,[3,4] have spawned intensive research into the magnetic properties of mesoscopic patterned elements, which have great potential for application in high-density storage and magnetoresistive random access memories (MRAM).[5,6] These elements also provide an ideal experimental system for studying fundamental physical issues; the magnetization switching mechanisms and domain configurations are of particular interest. In order to achieve a well-controlled and reproducible magnetic state, magnetic elements with different shapes, such as squares,[7] ellipses,[8,9] and disks,[10–12] have been studied. It has been shown that magnetic rings are a promising candidate[13–18] due to their tendency to form a flux-closure vortex state; this state is stable and features minimal interaction between adjacent elements because of the absence of stray field. Small ring structures generally exhibit three different domain configurations at remanence: the head-to-head and tail-to-tail "onion" state, the vortex state, and the single-domain state. The actual remanent state and transition between saturated states depends on the competition between magnetostatic energy and exchange energy, and anisotropy plays an important role. A recent study[18] on wide epitaxial Co rings found a direct transition between positive and negative single-domain states without any intermediate vortex state for rings with strong anisotropy. However, the behavior of narrow rings remains unclear and will be the subject of this study.

Magnetic force microscopy (MFM) has become the most commonly-used tool to study local magnetic structure and magnetization reversal because of its high resolution and versatility. The problems with MFM are that local field emanating from the magnetized tip can interact with and distort the magnetic structure of the sample, and that only the gradient of stray field can be detected. These issues complicate the interpretation of data.[9] Recently, a number of imaging tools have been developed to noninvasively image magnetic samples, such as scanning electron microscopy with polarization analysis (SEMPA)[12] and scanning Hall probe microscopy (SHPM).[19] Of these, scanning magnetoresistive microscopy (SMRM)[20] seems to be the most promising one. This technique utilizes a submicron-resolution magnetoresistive (MR) sensor[21] to image magnetic fields at the sample surface. The sensor readout is directly proportional to the vertical (z) component of local stray field. Compared to MFM, the SMRM technique has two notable advantages: the sensor has little effect on the magnetic state of sample, and the absolute value of stray field from the sample can be measured, making analysis more straightforward.

In this paper, we use SMRM along with MFM to image remanent states in narrow micrometer-size Co polycrystalline rings with uniaxial anisotropy. We are particularly concerned with the details of magnetization reversal and with domain configurations of intermediate states, and their dependence on anisotropy. Our results show strong magnetic and structural changes upon introduction of a uniaxial anisotropy after thermal annealing in a field. The results can be understood via micromagnetic simulations.

II. EXPERIMENTAL DETAILS

Arrays of 10×10 rings were defined by electron-beam lithography at 30 keV beam energy on a Si substrate covered by a thermally grown oxide. After development, Co rings were obtained by depositing a polycrystalline tri-layer of Ti(50 Å)/Co(340 Å)/Pt(50 Å) using electron-beam evaporation followed by lift-off in acetone. Finally, a thin layer of SiO_2 (1000 Å) was sputtered onto the samples for further protection. The rings examined in this experiment had a width of 0.5 μm with outer diameters of 4 μm. The spacing between rings in each array is twice the diameter of the rings to minimize any magnetostatic coupling between rings. Morphology observations were conducted by scanning electron microscopy (SEM) and atomic force microscopy (AFM). Figure 1 shows SEM images of the ring array. In order to compare the effects of anisotropy on the magnetization of rings, some samples were annealed in a field of 1.6 kOe at 200 °C for about 10 min in ambient condition, to introduce a uniaxial anisotropy. The structural and magnetic properties of both types of rings were examined by AFM and MFM.

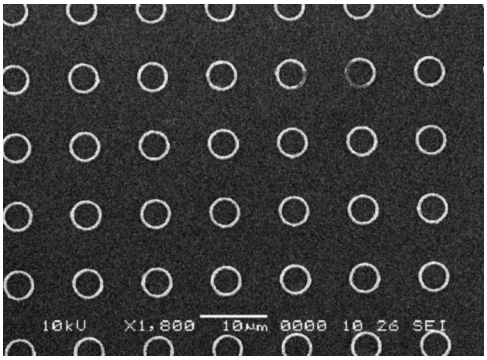

FIG. 1. Scanning electron micrographs of polycrystalline Co ring samples.

These images were collected with a Digital Instruments Dimensional III in tapping mode, i.e., monitoring the resonant frequency of the cantilever while the tip scans the sample at a fixed height.

Many details of magnetic imaging with SMRM have been described in a previous work.[20] The sensing probe was a commercial giant magnetoresistive read/write head used in IBM Travelstar 7200 drive sensor with submicron resolution. The microscope operates with the sensor and sample in light physical contact, and the probe is raster-scanned across the surface to detect stray fields emanating from the patterned rings. The effective distance between sensor and sample is about 0.2–0.3 μm, which sets a limit on the spatial resolution of the technique. Before putting on a new sensor head, a current-carrying test wire sample with known stray field value is first scanned at same height to resolve the sensor sensitivity. In this way, the absolute stray field value on unknown sample is obtained. For optimal signal-to-noise ratio (SNR), custom-made electronics based on lock-in amplification techniques, are utilized. In this way, low-frequency noise of the electronics is avoided without a loss in signal quality. Using this method, we have achieved SNR$>$46 dB.

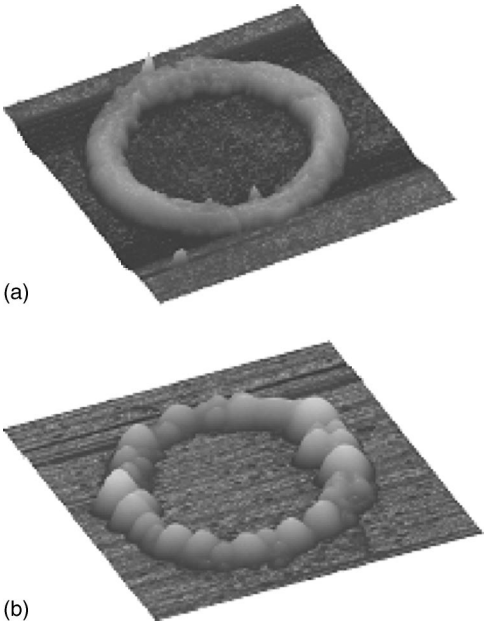

FIG. 2. AFM images of 4-μm Co rings (a) before and (b) after annealing. A significant enhancement in grain size is seen after annealing.

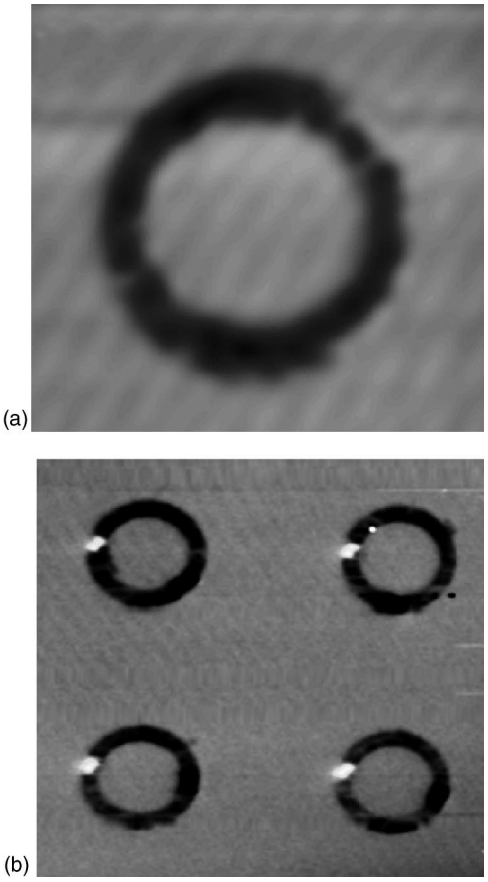

FIG. 3. MFM images of Co rings in the remanent state for samples (a) without and (b) with thermal annealing in a field.

III. RESULTS AND DISCUSSION

Figures 2(a) and 2(b) show typical AFM images of a ring before and after thermal annealing. Both images reveal some structural asymmetry and roughness, and some protrusions due to incomplete lift-off are also observed. These inhomogeneities may serve as domain pinning sites, increasing the likelihood of a complicated intermediate magnetic state. Figure 2 shows that thermal annealing has greatly changed the grain structure of the ring: the grain size of about 30–60 nm for as-deposited samples is dramatically increased to about $\sim$500 nm after annealing. As can be seen, the grain size is equal to the width of the rings in (b).

Figure 3 shows MFM images of rings at remanence before and after annealing. A tip coated with low-moment material (CoPtCr) was used to minimize the influence of tip stray field, in addition to the use of a relatively large lift height (150 nm). In as-deposited samples, a magnetic vortex structure was observed, as indicated by a weak contrast in Fig. 3(a). For annealed samples, however, MFM images indicate different magnetic configurations. The strong contrast signifies an onion state, which is characterized by points of

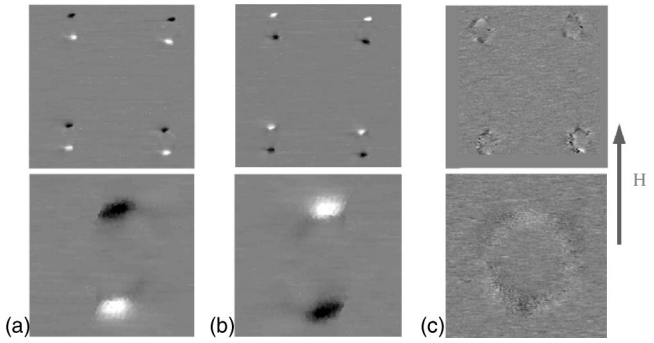

FIG. 4. A sequence of SMRM images, measured in the absence of field, for as-deposited samples after exposure to differing magnetic field values: (a) 1000 Oe, (b) −500 Oe, and (c) −250 Oe. Bottom row is the corresponding images of individual ring. The image contrast in (a) and (b) is normalized to same field scale (+/−80 Oe), whereas the contrast in (c) is normalized to (+/−10 Oe). The arrow on the right shows the applied field direction (positive) before each scan.

dark and light contrast at opposite positions on the ring; these magnetic signatures originate from two domain walls. These states were observed in all samples examined, although the pole locations varied somewhat, most likely due to defects in individual rings.

The magnetic domain structure of rings and their stray-field distribution were further investigated with SMRM. In order to minimize system noise originating from an in-situ magnetic field, all data are presented at remanence. The experiment was performed by first saturating the rings in a field of 1000 G, and then reversing the field direction in steps. Between steps, the samples were taken out of the applied field and imaged with SMRM. This process was continued until a full reversal of magnetization was observed for all rings. As an example, Fig. 4 is a series of images showing the progression of magnetic states in as-deposited samples as imaged by SMRM. The data have been scaled linearly, with bright regions representing the largest positive stray fields and dark regions representing the most negative stray fields. All field value is obtained using precalibrated sensor sensitivity. The results from Fig. 4 are unsurprising: after saturation, all rings are in onion states, confirmed by a strong dipole-like stray field signal, with a measured amplitude of up to 75 Oe [Fig. 4(a)]. When the field direction is reversed and the amplitude increased in the opposite direction, the rings switch to a reversed onion state [Fig. 4(b)] via an intermediate vortex state [Fig. 4(c)] as indicated by a much lower contrast compared to onion state. At a field of 500 Oe, over 80% of rings have switched to the final reversed onion states. It should be noted that even though the vortex state should be flux-closed and exhibit no contrast in image, considerable stray field (∼6 G) was detected for some rings in this state. This finding can be attributed to sample surface roughness and microstructural variation, which may locally pin domain walls.

We are most interested in the magnetic behavior of rings after thermal annealing; in particular, the effects of uniaxial anisotropy on magnetization switching. Annealed samples were imaged using the same procedure just described, and

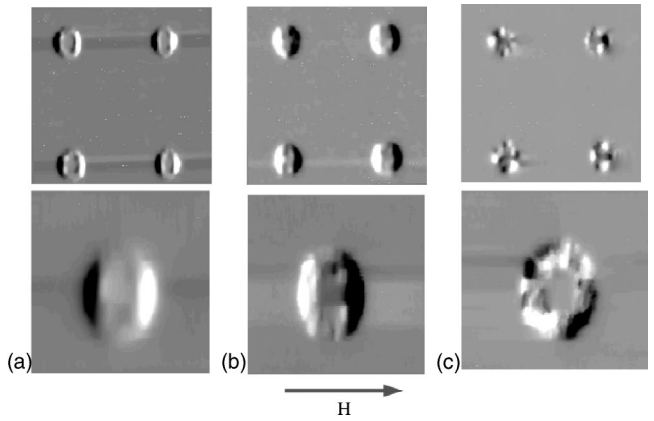

FIG. 5. SMRM images of annealed samples after exposure to varying magnetic fields along the easy-axis direction: (a) 1000 Oe, (b) −500 Oe, and (c) −300 Oe. Bottom row is the corresponding images of individual ring. The image contrast in (a) and (b) is normalized to same field scale (+/−80 Oe), whereas the contrast in (c) is normalized to (+/−30 Oe). The arrow on the bottom shows the applied field direction (positive) before each scan.

the results are shown in Fig. 5. Annealed rings undergo the same onion-to-reverse-onion transition [Figs. 5(a) and 5(b)], with peak-to-peak stray fields of 150 Oe in each case, but the dark-bright contrast in onion states is much broader than that of unannealed rings in the same state. These images cannot be understood as resulting from single-domain states because in that case, we would expect a dark-bright-dark-bright field pattern due to accumulation of stray magnetic static charge at both the inner and outer diameter of the ring. This pattern is never observed in any of the rings. We hypothesize that this broadening is partially due to the increase in grain size (Fig. 2) after annealing. Anisotropy induced by annealing also plays an important role, as it tends to align spins along the easy axis, resulting in a thick domain wall.

In contrast to as-deposited samples, the transition from the onion to the reverse-onion state is not accompanied by an intermediate vortex state in annealed rings. A detailed study of the full switching process by SMRM shows that the initial onion state is stable up to a field of ∼−150 G, after which it evolves (∼−200 G) into a complex multidomain state by nucleation. This state [Fig. 5(c)] is indicated by alternating positive and negative field poles, although the position and distribution of each pole are different in each ring. The stray field magnitude for this state is ∼60 Oe peak-to peak. This configuration persists until an applied field of roughly −400 G, at which rings begin to favor the reversed onion state. At a field of −400 G, all rings have completely switched [Fig. 5(b)]. Never at any stage was a completely flux-closed state observed. The significant differences in the switching process for rings with and without annealing confirm a strong dependence of switching behavior on anisotropy.

IV. MICROMAGNETIC SIMULATIONS

Micromagnetic simulations were carried out to gain further understanding into the reversal mechanism in rings with

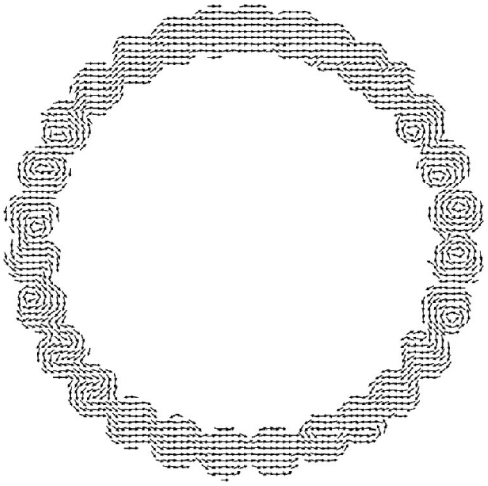

FIG. 6. Micromagnetic simulation results showing the magnetization configuration of the intermediate state for a Co ring with uniaxial anisotropy.

strong anisotropy. We used the OOMMF 2D micromagnetic simulation package developed at NIST[22] to calculate equilibrium magnetization configurations at different fields. The cell size for each simulation was 5×5 nm with a cell height identical to the film thickness (34 nm). The ring morphology was specifically designed to have multiple grains with a size comparable to the ring width to incorporate the observed enhancement of grain size and variation in microstructure after annealing. The simulations showed a noncoherent buckling-like reversal process in the grains near the domain walls, which induces nonuniform magnetization. The switching process starts with nucleation of local vortices at the domain edges, followed by successive formations of vortices in adjacent grains. The size of these local vortices is comparable to the grain size. Figure 6 depicts a typical magnetic configuration in this intermediate state. Adjacent vortex structures tend to have opposite directions of rotation, leading to alternating out-of-plane stray fields at successive cores. This alternating contrast in nearby domains is confirmed in many SMRM images [see Fig. 5(c)]. Identical behavior was observed in rings with uniform morphology, proving that this reversal mechanism is insensitive to structural inhomogeneities. Our simulations predict that, at some critical field, the top and bottom regions of the ring reverse instantaneously via coherent rotation, without local vortex formation. However, this dynamic behavior was not confirmed experimentally, because our setup can only resolve states which are at least metastable. It should be noted that the relatively low annealing temperature makes it likely that the induced anisotropy is less than that of epitaxial Co ($K\approx500{,}000$ J/m^3 for hcp Co). By comparing experimental and simulated switching fields, we have found that an anisotropy value of $30{,}000$ J/m^3 is most consistent with our observations.

We also simulated rings without annealing, making the assumption of zero anisotropy. The results were unsurprising and agree with previous findings:[14] the magnetization in unannealed rings switches from one onion state to the other through a global vortex state. The transition into this vortex state takes place via movement of one domain wall, with the other exhibiting little or no movement, until the two walls meet and annihilate.

Li *et al.*[18] explored the possible reasons why a ring with strong anisotropy cannot support a vortex state. They concluded that when the anisotropy strength exceeds a critical value ($10\,000$ J/m^3), the vortex state is rendered unstable, which agrees with our results. However, they saw an irreversible transition between saturated states, with no intermediate states, for epitaxial rings with very strong anisotropy. In contrast, we have observed the existence of a complicated multidomain intermediate configuration for our annealed samples with relatively moderate anisotropy. It is reasonable that this state is a new metastable phase that is only energetically favorable for a middle range of anisotropies. The competition between anisotropy energy and demagnetization energy naturally favors a vortex state for sufficiently small anisotropies, with the aforementioned configuration becoming favorable for larger anisotropies. In-situ SMRM imaging, along with simulations, for rings with different annealing conditions, and hence different induced anisotropies, will be conducted to further explore the behavior of this system. For imaging in an applied field, the stray field of an MFM tip can be sufficient to disrupt the magnetic state of the sample, particularly for configurations that persist only over narrow field ranges. Therefore, we believe that SMRM has distinct advantages for this type of in-situ study.

V. CONCLUSIONS

In summary, we have imaged the magnetization reversal process of narrow Co rings by imaging their remanent states using SMRM. This technique is noninvasive and provides direct information about sample magnetization. We have observed a complicated multidomain intermediate phase during the transition between onion states for samples annealed in a field. Micromagnetic simulations have shown that switching occurs through a noncoherent vortex buckling process combined with coherent rotation. This is in contrast to as-deposited samples, which reverse by simple domain wall motion and feature an intermediate vortex state.

ACKNOWLEDGMENT

This work was supported by the National Science Foundation Grant Nos. DMR-0071770 and DMR-0074080.

[1] S. Y. Chou, Proc. IEEE **85**, 652 (1997).
[2] C. A. Ross, H. I. Smith, T. Savas, M. Schattenburg, M. Farhoud, M. Hwang, M. Walsh, and R. J. Ram, J. Vac. Sci. Technol. B **17**, 3168 (1999).
[3] Y. Chen, A. Lebib, S. P. Li, M. Natali, D. Peyrade, and E. Cambril, Microelectron. Eng. **57–58**, 405 (2001).
[4] S. Y. Chou, P. R. Krauss, and P. J. Renstrom, Appl. Phys. Lett. **67**, 3114 (1995).
[5] S. A. Wolf, D. D. Awschalom, R. A. Buhrman, J. M. Daughton, S. von Molnar, M. L. Roukes, A. Y. Chtchelkanova, and D. M. Treger, Science **294**, 1488 (2001).
[6] J. G. Zhu, Y. F. Zheng, and G. A. Prinz, J. Appl. Phys. **87**, 6668 (2000).
[7] R. P. Cowburn, A. O. Adeyeye, and M. E. Welland, Phys. Rev. Lett. **81**, 5414 (1998).
[8] P. Vavassori, O. Donzelli, L. Callegaro, M. Grimsditch, and V. Metlushko, IEEE Trans. Magn. **36**, 2993 (2000).
[9] X. Zhu, P. Grutter, V. Metlushko, and B. Ilic, Phys. Rev. B **66**, 024423 (2002).
[10] T. Shinjo, T. Okuno, R. Hassdorf, K. Shigeto, and T. Ono, Science **289**, 930 (2000).
[11] M. Hehn, K. Ounadjela, J. Bucher, R. Rousseauz, D. Decanini, B. Bartenlian, and C. Chappert, Science **272**, 1782 (1996).
[12] C. A. F. Vaz, L. Lopez-Diaz, M. Klaui, J. A. C. Bland, T. L. Monchesky, J. Unguris, and Z. Cui, Phys. Rev. B **67**, 140405 (2003).
[13] Y. G. Yoo, M. Klaui, C. A. Vaz, L. J. Heyderman, and J. A. C. Bland, Appl. Phys. Lett. **82**, 2470 (2003).
[14] J. Rothman, M. Klaui, L. Lopez-Diaz, C. A. F. Vaz, A. Bleloch, J. A. C. Bland, Z. Cui, and R. Speaks, Phys. Rev. Lett. **86**, 1098 (2000).
[15] F. J. Castano, C. A. Ross, C. Frandsen, A. Eilez, D. Gil, H. I. Smith, M. Redjdal, and F. B. Humphrey, Phys. Rev. B **67**, 184425 (2003).
[16] M. Klaui, J. Rothman, L. Lopez-Diaz, C. A. F. Vaz, J. A. C. Bland, and Z. Cui, Appl. Phys. Lett. **78**, 3268 (2001).
[17] S. P. Li, D. Peyrade, M. Natali, A. Lebib, Y. Chen, U. Ebels, L. D. Buda, and K. Ounadjela, Phys. Rev. Lett. **86**, 1102 (2003).
[18] S. P. Li, W. S. Lew, J. A. C. Bland, M. Natali, A. Lebib, and Y. Chen, J. Appl. Phys. **92**, 7397 (2002).
[19] J. Bekaert, D. Buntinx, C. Van Haesendonck, V. V. Moshchalkov, J. De Boeck, G. Borghs, and V. Metlushko, Appl. Phys. Lett. **81**, 3413 (2003).
[20] B. D. Schrag and G. Xiao, Appl. Phys. Lett. **82**, 3272 (2003).
[21] H. Tsang, R. E. Fontana, T. Lin, D. E. Heim, B. A. Gurney, and M. L. Williams, IBM J. Res. Dev. **42**, 103 (1998).
[22] The micromagnetic simulation package (OOMMF) is available at http://math.nist.gov/oommf